https://doi.org/10.5194/esd-2019-94
Preprint. Discussion started: 2 April 2020

Earth System Dynamics Discussions

Biases in the albedo sensitivity to deforestation in CMIP5 models and their impacts on the associated historical Radiative Forcing

Quentin Lejeune[1,2], Edouard L. Davin[2], Grégory Duveiller[3], Bas Crezee[2], Ronny Meier[2], Alessandro Cescatti[3], Sonia I. Seneviratne[2]

[1]Climate Analytics, Berlin, 10969, Germany
[2]Institute for Atmospheric and Climate Science, ETH Zurich, Zurich, 8092, Switzerland
[3]European Commission Joint Research Centre, Ispra (VA), 21027, Italy

Correspondence to: Quentin Lejeune (quentin.lejeune@climateanalytics.org)

Abstract. Climate model biases in the representation of albedo variations between land cover types contribute to uncertainties on the climate impact of land cover changes since pre-industrial times, and especially on the associated Radiative Forcing. The recent publications of new observation-based datasets offer opportunities to investigate these biases and their impact on historical albedo changes in simulations from the fifth phase of the Coupled Model Intercomparison Project (CMIP5). Conducting such an assessment is however complicated by the non-availability of albedo values for specific land cover types, as well as the limited number of simulations isolating the land use forcing in CMIP. In this study, we demonstrate the suitability of a new methodology to extract the albedo of trees and crops/grasses in standard climate model simulations. We then apply it to historical runs from 13 CMIP5 models and compare the obtained results to satellite-derived reference data. This allows us to identify substantial biases in the representation of the albedo of trees, crops/grasses, and the albedo change due to the transition between these two land cover types in the analysed models. Additionally, we reconstruct the local albedo changes induced by historical conversions between trees and crops/grasses for 15 CMIP5 models. This allows us to derive estimates of the Radiative Forcing from albedo variations due to land cover changes since pre-industrial times ranging between 0 and -0.22 W/m^2, with a mean value of -0.07 W/m^2. Constraining the albedo response to transitions between trees and crops/grasses from the models with satellite-derived data leads to an increase in this range, however after excluding two models with unrealistic conversion rates from trees to crops/grasses we obtain a revised model mean estimate of -0.11 W/m^2 (with individual model results between -0.04 and -0.16 W/m^2). These numbers are at the lower end of the range provided by the IPCC AR5 (-0.15 +/- 0.10 W/m^2). The approach described in this study can be applied on other model simulations, such as those from CMIP6, especially as a diagnostic enabling the reproduction of the model evaluation part has been included in the ESMValTool v2.0.

https://doi.org/10.5194/esd-2019-94
Preprint. Discussion started: 2 April 2020


Earth System Dynamics Discussions

1 Introduction

The landscape transformations imposed by anthropogenic activities have the potential to modify the climate (Foley *et al.*, 2005; Mahmood *et al.*, 2014). Since pre-industrial times, important Land Cover Changes (LCC) have especially led to the replacement of forests by shorter vegetation types such as crops and grasses over large inhabited areas (Ramankutty and Foley, 1999; Pongratz *et al.*, 2008; Hurtt *et al.*, 2011; Kaplan *et al.*, 2011). Associated alterations of land surface properties such as albedo, roughness and evaporative fraction have modified climate conditions through the so-called biogeophysical effects (Pongratz *et al.*, 2010; de Noblet-Ducoudré *et al.*, 2012; Lejeune, Seneviratne and Davin, 2017). The overall climate impact of the biogeophysical effects of historical LCC remains a matter of debate (Pitman *et al.*, 2009; de Noblet-Ducoudré *et al.*, 2012; Lejeune, Seneviratne and Davin, 2017; Duveiller *et al.*, 2018) due to uncertainties regarding the magnitude of the imposed land-cover perturbations (Schmidt *et al.*, 2012), the resulting alterations in land surface properties, the interplay between radiative (related to albedo) and non-radiative processes (related to changes in evaporative fraction and roughness), and the influence of atmospheric feedbacks and non-local effects (Winckler, Reick and Pongratz, 2017; Winckler *et al.*, 2019).

Concerning the albedo more specifically, model studies concluded that historical LCC have led to large-scale increases in this variable (Betts *et al.*, 2007; Boisier *et al.*, 2013) because trees have a lower albedo than shorter vegetation types, especially in the presence of snow (Cescatti *et al.*, 2012; Li *et al.*, 2015). This has resulted in a cooling effect, and climate models have simulated an associated global Radiative Forcing (RF) close to -0.2 W/m^2 (Betts *et al.*, 2007; Edouard L. Davin, de Noblet-Ducoudré and Friedlingstein, 2007; Pongratz *et al.*, 2009). However, Myhre, Kvalevåg and Schaaf (2005) and Kvalevåg *et al.* (2010) have argued that climate models usually overestimate the albedo difference between natural vegetation and croplands in comparison to satellite-derived observational evidence. By combining a radiative transfer model with reconstitutions of past albedo changes based on satellite observations of the current vegetation land cover and its surface albedo, as well as a data set for potential natural vegetation, Myhre, Kvalevåg and Schaaf (2005) rather found a RF due to anthropogenic vegetation changes of -0.09 W/m^2 since pre-agriculture times. Consequently, the Fifth Assessment Report (AR5) of the IPCC estimated that LCC since 1750 have rather led to a RF of -0.15 +/- 0.10 W/m^2 (Myhre *et al.*, 2013). A substantial spread in the albedo response to historical LCC has also been identified amongst the models participating in the LUCID project (de Noblet-Ducoudré *et al.*, 2012). The diversity of model parameterisations was estimated to be responsible for about half of it, while the remaining uncertainties result from differences in the magnitude of the prescribed land cover.

More recent model intercomparison efforts such as the fifth phase of the Coupled Model Intercomparison Project (CMIP5, Taylor, Stouffer and Meehl, 2012) offer new opportunities to assess the magnitude of these model disagreements, as well as our understanding of the impact of historical LCC on albedo and the associated RF. Nevertheless, such an investigation is complicated by the facts that the modelling groups participating in CMIP5 have not provided data on the albedo of specific land-cover types but only mean albedo values over grid cells accounting for land cover heterogeneity, and that few of them

https://doi.org/10.5194/esd-2019-94
Preprint. Discussion started: 2 April 2020


Earth System Dynamics Discussions

have conducted experiments isolating the historical land use forcing. In parallel to recent model developments, studies giving insights from satellite data on the climate effect of LCC have been published (Li *et al.*, 2015; Alkama and Cescatti, 2016; Duveiller, Hooker and Cescatti, 2018b). They provide high-resolution information on the potential changes in various surface variables in response to land-cover transitions, which constitutes a very good benchmark to evaluate how this aspect is represented in climate models.

This study is divided in several parts. First, we introduce a new methodology to extract the albedo of two specific land cover classes (trees and crops/grasses) in simulations for which information is only available at the grid cell level (Section 2). Second, we evaluate how well this methodology performs by using as a testbed climate model simulations that also provide sub-grid cell albedo values for specific land-cover types (Section 3). Third, we apply this approach to CMIP5 simulations to extract the albedo of trees and crops/grasses, as well as the albedo change due to transitions between these land cover classes, and compare the obtained results to satellite-derived reference data (Section 4). Fourth, we reconstruct the albedo changes since preindustrial times in CMIP5 models, and calculate the associated RF (Section 5). We also discuss the spread in the obtained model results in light of the biases identified in the previous step, and apply an observational constraint based on satellite-derived evidence to refine our estimates of the RF from historical LCC. Eventually, we compare our findings to those of previous studies, and discuss their limitations as well as potential for follow-up analyses (Section 6).

2 Methods and Data

2.1 Observational data for the albedo of land-cover classes and the albedo changes associated to land-cover transitions

2.1.1 Albedo of land-cover classes

In this study we evaluate the simulated albedo of crops/grasses (merged into one single land cover class) and trees against reference estimates obtained from satellite measurements. To derive them, we used the 300 meter-resolution land cover information provided by GlobCover v2.3 (Arino *et al.*, 2012), collected between January 2005 and June 2006, in combination with the mean of the white-sky (bi-hemispherical) and black-sky (directional-hemispherical) shortwave albedo data at 0.05°-resolution from GlobAlbedo (Lewis *et al.*, 2012), available at monthly timescale for the 1998-2011 period. To extract the albedo from specific land-cover types at a resolution of 2° (i.e., comparable to that of the model simulations), the GlobCover original data were first regridded at 0.0025°. For each spatial grid cell of the GlobAlbedo dataset which is occupied by at least 95% by either trees or crops/grasses according to the GlobCover product, the seasonal cycle of albedo for this specific land cover type was then approximated by the monthly albedo climatology for this grid cell, computed over the full period covered by GlobAlbedo. The results are then aggregated at 2° resolution, i.e. for each 2° grid cell the albedo climatology of a specific land cover type is derived by calculating area-weighted averages over the 0.05°-resolution grid cells it contains, and for which a land cover-specific seasonal cycle of albedo was previously identified.

https://doi.org/10.5194/esd-2019-94
Preprint. Discussion started: 2 April 2020


Earth System Dynamics Discussions

2.1.2 Albedo changes associated to land-cover transitions

The dataset of Duveiller, Hooker and Cescatti (2018a) – thereafter referred to as D18 – was used to evaluate the albedo changes associated to land-cover transitions between trees and crops/grasses in CMIP5 models. This observational dataset was derived by "unmixing" the monthly albedo climatology over the 2008-2012 period from collection v005 of the NASA MCD43C3 product (Schaaf *et al.*, 2002), using land cover information for the year 2010 from the ESA-CCI land-cover dataset (ESA Land Cover CCI Product User Guide Version 2. Tech. Rep., 2017, available at: http://maps.elie.ucl.ac.be/CCI/viewer/download/ESACCI-LC-PUG-v2.5.pdf). Their methodology is based on a "space-for-time" analogy, i.e. it assumes that albedo changes that would arise from a land cover transition from trees to crops/grasses, for example, can be approximated by spatial differences between albedo values of trees and crops/grasses over neighbouring areas, which can therefore be assumed to experience similar background climates. We used the version of the dataset from D18 that is based on a generic vegetation classification (IGBPgen) in four land cover classes: trees, shrubs, crops/grasses and savannas.

The spatial coverage of the data from D18 is limited to the areas where there is a joint presence of the two vegetation classes of interest for a given land cover transition (e.g. forests to grasslands/croplands when considering a typical deforestation) over a local area of roughly 5 by 5 km. This is often not an issue, since many LCC generally occur in regions where both target and source classes already occur. However, it does limit the area over which the data can be confronted with model results, and it precludes exploring the possibilities of analysing new land cover change trajectories (e.g. planting trees in areas where none currently exist). Therefore, for the part of the analysis in which we estimate the observation-constrained RF associated to historical LCC in CMIP5 simulations, we used an extended version of the dataset originally presented by D18 that has a broader spatial coverage (Duveiller *et al.*, 2020). The gap-filling approach employed to derive it consisted in training a random forest classifier to reproduce the data according to similarities in local climate, and then using the climate information to predict the albedo changes due to specific land-cover transitions where gaps existed in the data. Some precautions were taken to ensure that these predicted outputs remain realistic. First, all areas in which neither of the two land cover types involved in a given transition are present were removed. Second, the random forest is only used for interpolation, i.e. only using combinations of climate indicator values that are actually observed for the considered transition. Finally, a clear systematic bias of the classifier was corrected by applying a simple linear regression.

2.2 Climate model simulations from CMIP5

We reconstruct the present-day albedo from trees as well as crops/grasses in the historical "all-forcings" simulations (Taylor, Stouffer and Meehl, 2012) of 13 CMIP5 models for which the required information on land cover, downwelling shortwave radiation, upwelling shortwave radiation and snow cover fraction is available (see Section 2.3.1 for a description of the reconstruction methodology). Land fractions covered by crops, grasses and pasture are provided separately by CMIP5

https://doi.org/10.5194/esd-2019-94
Preprint. Discussion started: 2 April 2020


Earth System Dynamics Discussions

models, but were grouped within one same land cover class for consistency with the observational data from D18. Present-day albedo values are extracted from the last five-year period common to all models (i.e., 2000-2004), to be as close as possible to the period covered by the observational data. If several ensemble members differing only in terms of their initial conditions were available for one specific model, the reconstruction method was applied to their ensemble mean.

In Section 5, we present estimates of the RF associated to historical deforestation in fifteen CMIP5 models. For this purpose, we first reconstruct the albedo changes associated with transitions between trees and crops/grasses between pre-industrial conditions (equivalent to those of 1860 in CMIP5 and extracted from the first 200 years of the "piControl" experiments), and the 1981-2000 time period of historical "all-forcings" experiments. The reconstruction algorithm is applied to all CMIP5 models for which the required information on land cover, downwelling and upwelling shortwave radiation is available for at least two ensemble members of the analysed experiments (see Section 2.3.2 for a description of the reconstruction methodology). In order to be able to compute the RF constrained by observations, both the reconstructed albedo changes associated with transitions between trees and crops/grasses and the data from D18 were regridded to 1°x1° resolution. We have focused on the transitions between trees and crops/grasses for consistency with the observational data of D18, but also assessed the sensitivity of our results when considering the historical impact of overall changes in tree cover (e.g., also including replacement of trees by shrubs or bare soil).

2.3 Principle of the reconstruction method

2.3.1 Reconstruction of the simulated present-day albedo of specific land-cover classes

The present-day albedo values from trees and crops and grasses (α_{tr} and α_{cg}) are reconstructed in CMIP5 historical simulations using an "unmixing" method similar to those previously applied to satellite-derived observational data to extract the land surface characteristics of specific land cover types (e.g., Alkama and Cescatti, 2016), including albedo (Li *et al.*, 2015; Chen and Dirmeyer, 2019), and notably to obtain the data from D18 used as a reference for the evaluation of CMIP5 models in this study. We include information on the land fraction covered by shrubs in the methodology, but do not reconstruct the albedo of this land cover type (α_{sh}) because of their limited spatial occurrence.

Concretely, for every land grid cell i we considered big boxes of a size of 5 times 5 grid cells centered over i. Within each big box, for each month we thus have a sample of up to 25 values for albedo (α) and the land cover fractions occupied by each of the three considered land cover classes (lcf_{tr}, lcf_{sh}, lcf_{cg}) over the same simulation period. Multi-linear regressions of α against lcf_{tr}, lcf_{sh} and lcf_{cg} are then performed in order to obtain α_{tr}, α_{sh} and α_{cg}.

https://doi.org/10.5194/esd-2019-94
Preprint. Discussion started: 2 April 2020


Earth System Dynamics Discussions
Open Access
EGU

Because snow cover has an important impact on albedo and especially on the albedo difference between forests and short vegetation types, two separated regressions are conducted for each big box: one among the grid cells with snow cover fraction inferior to 0.1 (considered as snow-free), and one for the grid cells where this variable is superior to 0.9 (considered as snow-covered):

$$\alpha^{sf} = \beta_0^{sf} + lcf_{tr} \times \beta_1^{sf} + lcf_{sh} \times \beta_2^{sf} + lcf_{cg} \times \beta_3^{sf} \quad (1)$$

$$\alpha^{sc} = \beta_0^{sc} + lcf_{tr} \times \beta_1^{sc} + lcf_{sh} \times \beta_2^{sc} + lcf_{cg} \times \beta_3^{sc} \quad (2)$$

where lcf_{tr}, lcf_{sh} and lcf_{cg} are vectors containing up to 25 values, the β coefficients are specific to each big box and each month, and the superscript *sf* and *sc* refer to snow-free and snow-covered, respectively.

α_{tr}, α_{sh} and α_{cg} over the central grid cell *i* of a big box are then computed by extrapolating the partial linear regression lines for cases where lcf_{tr}, lcf_{sh} or lcf_{cg} are equal to 100%:

$$\alpha_{tr}^{sf}(i) = \beta_0^{sf} + \beta_1^{sf} \times 100\% \quad (3)$$

$$\alpha_{sh}^{sf}(i) = \beta_0^{sf} + \beta_2^{sf} \times 100\% \quad (4)$$

$$\alpha_{cg}^{sf}(i) = \beta_0^{sf} + \beta_3^{sf} \times 100\% \quad (5)$$

$$\alpha_{tr}^{sc}(i) = \beta_0^{sc} + \beta_1^{sc} \times 100\% \quad (6)$$

$$\alpha_{sh}^{sc}(i) = \beta_0^{sc} + \beta_2^{sc} \times 100\% \quad (7)$$

$$\alpha_{cg}^{sc}(i) = \beta_0^{sc} + \beta_3^{sc} \times 100\% \quad (8)$$

The method can only perform well over big boxes with sufficient land cover information. Therefore, the predictors (lcf_{tr}, lcf_{sh}, lcf_{cg}) are only included in the regression if the respective land cover classes are represented in at least two snow-free or snow-covered grid cells. Moreover, the regressions are only conducted in the big boxes with a minimum number of 15 grid cells (either snow-free or snow-covered), and where the sum of all the included predictors exceeds 90%. Moreover, the few remaining reconstructed albedo values which are physically impossible (i.e., either inferior to 0 or superior to 1) are filtered out. As a last step to increase the quality of the results of the reconstruction method, grid cells for which the standard error of the regression is higher than 0.01, or where the land fraction covered by trees and crops/grasses is lower than 20% are discarded. The albedo change associated to a transition between trees and crops/grasses is eventually derived by looking at the difference between the reconstructed albedo of trees and crops/grasses. The filtering criteria differ slightly in this case, as we only discard grid cells for which both the land fraction covered by trees and crops/grasses are lower than 10% and where the standard error of the regression is higher than 0.001 (as the fraction covered by trees and crops/grasses covary,

https://doi.org/10.5194/esd-2019-94
Preprint. Discussion started: 2 April 2020

when looking at the reconstructed difference between the albedo of these land cover types the standard error of the regression strongly decreases). A diagnostic has also been implemented in the ESMValTool v2.0, which allows the automated application of the reconstruction methodology described in this section to simulations following a similar output protocol as CMIP (more details available in Eyring *et al.*, 2019).

2.3.2 Reconstruction of the simulated albedo changes due to historical deforestation

A similar approach based on local regression is used to derive the albedo changes associated to transitions between trees and crops/grasses between pre-industrial times and the 1981-2000 period ($\delta\alpha_{tr\rightarrow cg}$). It has previously been used to reconstruct local changes in temperature due historical LCC in CMIP5 simulations (Lejeune *et al.*, 2018). In this case, the spatial predictors used in the regression are the historical transition rate between trees and crops and grasses ($lcc_{tr\rightarrow cg}$), latitude (lat), longitude (lon), and elevation ($elev$), such that:

$$\delta\alpha_{tr\rightarrow cg} = \delta_0 + lcc_{tr\rightarrow cg} \times \delta_1 + lat \times \delta_2 + lon \times \delta_3 + elev \times \delta_4 \quad (9)$$

where $lcc_{tr\rightarrow cg}$, lat, lon and $elev$ are vectors containing up to 25 values and the δ coefficients are specific to each big box. The historical albedo change associated to historical, local deforestation over the central grid cell i of a big box is then obtained by scaling the results of this local regression with the historical conversion rate from trees to crops/grasses experienced over i (compared with pre-industrial conditions):

$$\delta\alpha_{tr\rightarrow cg}(i) = lcc_{tr\rightarrow cg}(i) \times \delta_1 \quad (10)$$

We reconstruct $\delta\alpha_{tr\rightarrow cg}$ over each land grid cell for which the corresponding big box contains at least 15 land grid cells. An uncertainty range for $\delta\alpha_{tr\rightarrow cg}$ is also computed by applying the regression to each ensemble simulation of a given model. Additionally, for each ensemble simulation and each big box, a jackknife resampling is conducted: Alternatively, and as many times as there are land grid cells with non-missing values in the big box, an additional regression is computed after leaving out one grid cell (Efron, 1982). We thus obtain between 16 and 26 estimates of $\delta\alpha_{tr\rightarrow cg}$, depending on the number of land grid cells in the big box. We then retain the median of these estimates, which increases the robustness of our results by eliminating strong dependencies on single model grid cells.

2.4 Computation of the Radiative Forcing of historical conversions between trees and crops/grasses

The Radiative Forcing (RF), expressed here in W/m^2, is defined as the net change in the energy balance of the Earth system due to some imposed perturbation (Myhre *et al.*, 2013). In our case, this perturbation is a modification of albedo arising from

https://doi.org/10.5194/esd-2019-94
Preprint. Discussion started: 2 April 2020


Earth System Dynamics Discussions

land-cover changes, in particular deforestation or re/afforestation, which affects the amount of reflected shortwave radiation leaving the Earth system at the top of the atmosphere. By how much this amount changes depends on a so-called radiative kernel (Soden *et al.*, 2008), defined in this case as the differential response in outgoing shortwave radiation at the top of the atmosphere to an incremental change in surface albedo $\delta\alpha_s$ (Bright and O'halloran, 2019):

$$RF = K_{\alpha_s} \times \delta\alpha_s \quad (11)$$

We employ here the empirical parameterisation of the radiative kernel K_{α_s} suggested by Lenton and Vaughan (2009) and Cherubini, Bright and Strømman (2012), who approximate it as a combination of incoming shortwave radiation at the surface $SW_s^{\downarrow}$ and a temporally and spatially invariant one-way atmospheric transmittance k:

$$RF = SW_s^{\downarrow} \times k \times \delta\alpha_s \quad (12).$$

In this study, $SW_s^{\downarrow}$ is obtained from the edition 4a of the CERES-SYN1deg dataset (Wielicki et al., 1996), using the monthly climatology (over the 2001-2016 period) of its 1°-resolution product. We employ the value of 0.854 for k, as previously suggested by Lenton and Vaughan (2009) following the clear-sky results of a radiative transfer model used by Lacis and Hansen (1974). The RF associated to historical conversions between trees and crops/grasses can thus be written as follows:

$$RF_{tr \to cg} = 0.854 \times SW_s^{\downarrow} \times \delta\alpha_{tr \to cg} \quad (13)$$

We derive two types of RF estimates in the analysed CMIP5 models. For the first one ("unconstrained"), which is purely model-based, we used the $\delta\alpha_{tr \to cg}$ from historical conversion rates between trees and crops/grasses that were derived using the reconstruction method described in Section 2.3.2. The second one is constrained by observations, and was computed by combining the LCC implemented in the models and the albedo change associated to a transition between trees and crops/grasses from D18 to obtain $\delta\alpha_{tr \to cg}$.

2.5 Additional simulations to evaluate the reconstruction method

In order to evaluate the ability of the reconstruction method presented in Section 2.3.1 to extract the simulated albedo of trees and crops/grasses, we apply it to additional offline simulations conducted with the Community Land Model version 4.5 (CLM4.5; Oleson *et al.*, 2013) and compare its results to the subgrid signal of the respective land cover change (e.g., Malyshev *et al.*, 2015; Meier *et al.*, 2018). The simulations were conducted at 1.9°x2.5° resolution, forced by the CRUNCEP v4 atmospheric forcing dataset (Harris *et al.*, 2014) for the years 1997 to 2010, neglecting the first five years from the analysis. The default land cover map of CLM4.5 was kept constant at the state of 2000 throughout the simulation period (Lawrence and Chase, 2007). Grid cells in CLM4.5 are divided into tiles of different land units (glacier, wetland, vegetated,

https://doi.org/10.5194/esd-2019-94
Preprint. Discussion started: 2 April 2020


Earth System Dynamics Discussions

lake, and urban). The vegetated land unit comprises tiles of different Plant Functional Types (PFTs), including several types of trees, shrubs, grasses and crops, all receiving the same atmospheric forcing. We analyse tile-level model output to extract a subgrid albedo value for each land cover class (trees or crops/grasses). For each pixel and each month, the albedo values for the different land cover classes are computed as the area weighted means albedo across each PFT pertaining to the respective class over the simulation period. This reference value, later referred to as "subgrid" estimate, can then be compared to the reconstructed albedo values. The results of this evaluation are described in Section 3.

3 Evaluation of the methodology to reconstruct the albedo of individual land cover classes

3.1 Reconstruction of the albedo of trees and crops/grasses

The reconstructed July albedo estimates of trees and crops/grasses are close to the subgrid reference values in the CLM4.5 simulations, for the grid cells where the reconstruction method yields results (Figure 1). The main patterns of the spatial variability of the albedo of both land cover classes of interest, such as their latitudinal variations, are captured by the reconstruction method. The "error" of the reconstruction is shown by the differences between the reconstructed and subgrid albedo estimates, thus a global Root Mean Square Error (RMSE) can be computed across all grid cells for which a reconstructed estimate could be derived. For the month of July, the global RMSE equals 0.009 in the case of trees and 0.010 for crops/grasses (Table 1). Locally, the error is higher over some areas with stronger albedo gradients such as Western Europe, the Southeastern United States in the case of trees or Western Russia in the case of crops/grasses. Nevertheless, the absolute error rarely exceeds ~0.03, or ~20% of the subgrid values over these regions (Figure S1).

In January, the reconstructed albedo estimates still resemble closely the reference values from the subgrid model outputs (Figure 2), although the global RMSEs are higher (0.019 for trees, and 0.013 in the case of crops/grasses, see Table 1). These higher errors are due to the presence of snow over larger areas, which leads to increases in both the mean value and the spatial variability of albedo. As a result, within one big box used for the reconstruction, the dispersion between the albedo values from individual grid cells is higher. This renders the extraction of the correct albedo values of specific land cover classes with the regression-based reconstruction method more difficult. The spatial coverage of the reconstruction method also diminishes during months with a higher snow cover, because our methodology excludes grid cells which are neither considered snow-free nor snow-covered from the reconstruction, as is the case in Western Europe or the Northeastern United States in January. The absolute error of the reconstruction method reaches a maximum of ~0.1 or ~30-40% over localised parts of Eastern Siberia during this month (Figure S2).

Overall, the reconstruction method yields estimates of the albedo of trees and crops/grasses which are similar to the subgrid reference values in the analysed CLM4.5 simulations. This suggests that the reconstruction method can be applied to model runs produced with CMIP5 models, in order to estimate the albedo that they simulate for both of these land cover classes during present-day, and eventually compare it with observational reference data.

https://doi.org/10.5194/esd-2019-94
Preprint. Discussion started: 2 April 2020

295

3.2 Reconstruction of the albedo change from deforestation

Overall, the reconstructed estimates of the July albedo change associated to deforestation also show a good correspondence with the subgrid reference values (Figure 3). The global RMSE increases up to 0.019 in this case, because it is a combination of the errors associated to the reconstruction of the albedo of both trees and crops/grasses. The magnitude of this error needs
300 to be assessed in relation to the local albedo difference between albedo and crops/grasses. Previous studies using satellite observations have shown that this difference roughly ranges between 0.03 and 0.07 over mid-latitudes during summer (Li *et al.*, 2015; Duveiller, Hooker and Cescatti, 2018b). As a result, the local difference between the reconstructed and subgrid estimates can be as large as the overall albedo difference between forest and crops/grasses in some regions such as Western Europe or the Northeastern United States (Figure S3).

305 For January, the reconstructed and subgrid estimates of the deforestation-induced albedo change remain similar (Figure 4), with a global RMSE that slightly increases to 0.025 (Table 1). The relative error between the reconstructed and subgrid albedo values can reach 80% over localised tropical or subtropical areas, however it mostly remains limited to +/-10% over snow-covered regions (Figure S4). This is because the absolute error remains of similar magnitude as in snow-free regions, while the albedo change induced by deforestation increases in the presence of snow due to the snow-masking effect of
310 forests.

Overall, these results suggest that the reconstruction method can be applied in order to estimate the simulated deforestation-induced albedo change in CMIP5 models; however the interpretation of the results should be conducted with caution, keeping in mind the magnitude of the error associated to the reconstruction, especially over snow-free regions.

315

4 Present-day potential albedo changes associated to a transition from trees to crops/grasses in CMIP5 models and observations

4.1 Evaluation of the present-day albedo of trees and crops/grasses in CMIP5 models

4.1.1 Albedo of trees

320 The reconstructed albedo of trees varies considerably across the analysed CMIP5 models for the month of July, especially over the mid-to-high latitudes (Figure 5). Estimates derived from CanESM2 and the models from the MPI suite (MPI-ESM-LR, MPI-ESM-MR, MPI-ESM-P) show the highest similarities with those obtained by combining the observational datasets GlobAlbedo and GlobCover. The climate models which use the CLM as a land surface scheme (CCSM4, CESM1-CAM5, CESM1-FASTCHEM, CESM1-WACCM, NorESM1-M, NorESM1-ME) as well as MIROC5 all underestimate the albedo
325 of trees over mid-to-high latitudes. They indeed simulate values inferior to 0.1, whereas the estimates derived from observational data always remain above 0.1, and mostly range between 0.12 and 0.16 over these regions. The magnitude of the underestimation is in that case significantly higher than the reconstruction error which has been assessed from the analysis of the CLM4.5 simulations (global RMSE of 0.009, see Section 3.1). Lastly, our results indicate strong spatial

https://doi.org/10.5194/esd-2019-94
Preprint. Discussion started: 2 April 2020


Earth System Dynamics Discussions

variations in the case of the MIROC-ESM and MIROC-ESM-CHEM models, with negative biases over the high latitudes and Southeast Asia.

For January, observations show that the albedo of trees increases over the regions where snow is present (Figure 6). A latitudinal gradient can especially be noted, as the values derived from GlobCover and GlobAlbedo typically barely exceed 0.15 in Western Europe, but are higher than 0.3 in Scandinavia and even reach ~0.5 in Northern Siberia. Our results show that CanESM2 and the climate models using the CLM also simulate higher albedo values over snow-covered regions, with values that remain within the range indicated by observations for this time of the year. On the other hand, MIROC5 tends to overestimate albedo under the presence of snow, with values exceeding 0.5 north of ~50°N, and even reaching ~0.7 in areas located close to the Arctic ocean. Unfortunately, in the case of MIROC-ESM, MIROC-ESM-CHEM and the models from the MPI suite the spatial coverage of the reconstruction method is too low to be able to draw meaningful comparisons with observations over snow-covered areas.

4.1.2 Albedo of crops/grasses

There are also important variations among the simulated albedo of crops and grasses in the CMIP5 models we have analysed, pointing to significant model biases in comparison to observation-derived reference estimates. Overall, the models that employ the CLM tend to underestimate this quantity over large parts of the tropics and the mid-latitudes in the Northern Hemisphere in July, with reconstructed albedo values of ~0.13-0.14 whereas observations rather indicate values of at least 0.15 and even approaching 0.25 over the Sahel and Central Asia (Figure 6). This discrepancy appears less pronounced over the tropical parts of Africa and America located in the Southern Hemisphere, despite the lower availability of observational estimates over these regions. Our results also reveal that MIROC5 more systematically underestimates the albedo of crops/grasses, which remain inferior to 0.15 worldwide in this model. In contrast, the models from the MPI suite simulate albedo values that are consistently superior to those of the observations, exceeding 0.2 over large regions of the world. Importantly, the reported differences between the reconstructed model estimates and the reference values from observations are significantly higher than the error of the reconstruction method derived from the analysis of the CLM4.5 simulations (0.01 in the case of crops/grasses for the month of July, see Section 3.1). The albedo values simulated by MIROC-ESM and MIROC-ESM-CHEM appear closer to the observational estimates over the regions where those are available. Lastly, the spatial coverage of the reconstruction is low in the case of CanESM2, which prevents drawing robust conclusions for this model.

Results for the month of January indicate that the models that include the CLM, as well as MIROC5 and those from the MPI suite all represent the increase in the albedo of crops/grasses over snow-covered areas which is indicated by observational estimates (Figure 8). The limited spatial coverage of the latter over the high latitudes however makes it difficult to evaluate whether the magnitude of this increase is correctly represented. Over the tropical regions, the models including the CLM simulate an opposite pattern compared to that shown for the month of July, namely an underestimation of the albedo of

https://doi.org/10.5194/esd-2019-94
Preprint. Discussion started: 2 April 2020


Earth System Dynamics Discussions

crops/grasses in the Southern Hemisphere but more realistic estimates in the Northern Hemisphere. This suggests that these models simulate too high variations of the annual cycle for this variable over tropical regions.

365

4.2 Evaluation of the albedo changes induced by a transition from trees to crops/grasses in CMIP5 models

The observational dataset from D18 indicates that deforestation leads to a higher local albedo over each region of the world it covers, with some spatial variations. In July, this increase is lowest (<0.01) over Eastern Asia and Southwestern Siberia, and highest (~0.1) over the western part of North America (Figure 8). Our reconstructions indicate that most of the analysed
370 CMIP5 models simulate the deforestation-induced albedo increase over most regions of the world. However, there are biases that are significantly higher than the error of the reconstruction method derived from its evaluation on CLM4.5 simulations (0.019 in July and 0.025 in January, see Section 3.2).

For the month of July, the CanESM2 and MIROC5 models show the closest resemblance to the observational reference data, although they overestimate the albedo increase due to deforestation over some regions such as Eastern Asia and the eastern
375 part of North America. As a result of their strong overestimation of the albedo of crops/grasses (see Section 4.1), the models from the MPI suite exhibit significant positive biases in the deforestation-induced albedo increases across the globe in July, with values reaching ~0.1 over large areas. Positive biases of a lower magnitude, although still significant, are also found over specific regions in the models using the CLM as a land surface scheme, consistently with the evaluation of the subgrid albedo difference in CLM4.5 of Meier *et al.* (2018). Over the mid-latitudes, this is due to the underestimation in the albedo
380 of trees, whereas it can be related to the too high albedo of crops/grasses over the tropical regions of the Southern Hemisphere for this time of the year. Lastly, the MIROC-ESM and MIROC-ESM-CHEM models exhibit a strong spatial variability in the reconstructed signals. Contrary to the observational data which consistently indicate an increase in albedo after deforestation, our estimates suggest that both of these models simulate the opposite behaviour over extensive areas of Central Asia, but also the eastern parts of Canada and the United States and south of 25°S in Africa, America and Western
385 Australia.

Compared to July, the observations of D18 for the month of January indicate a higher albedo increase following deforestation over the mid-to-high latitudes where snow is present, the magnitude of which is overestimated by ~0.05-0.1 by the CMIP5 models including the CLM (Figure 10). These models also consistently simulate a localised albedo decrease following deforestation over Eastern Europe, while this feature is not present in the observations. Strikingly, our results
390 suggest that the MIROC-ESM and MIROC-ESM-CHEM models simulate strong albedo decreases (inferior to -0.3) over large-snow covered regions at this time of the year, a behaviour that is in strong contradiction with what observational data indicate. In line with the overestimation of the albedo of trees over high latitudes represented by MIROC5, this model also simulates albedo decreases as a response to deforestation over parts of Europe.

395

5 Implications for the Radiative Forcing from historical deforestation

https://doi.org/10.5194/esd-2019-94
Preprint. Discussion started: 2 April 2020


Earth System Dynamics Discussions

Our reconstructions of the RF from transitions between trees and crops/grasses since preindustrial times indicate a large spread within the CMIP5 models which were considered in this analysis (Figure 11), with estimates of the global mean RF ranging between 0 and -0.22 W/m^2. This dispersion is due to differences in two factors across the models: their local albedo responses to a transition between trees and crops/grasses, and the historical conversion rates between these two land cover classes that the models simulate or prescribe (depending on whether they used a dynamic vegetation module or not). In Eq. (10), the former factor is represented by δ_1, and the latter by $lcc_{tr \to cg}$. Observation-constrained estimates of the RF from the historical conversion rates in CMIP5 models were obtained by replacing the reconstructed values of δ_1 by those from D18 (Figure 12, see also Sections 2.3.2 and 2.4 for more information on the methodology). The differences between the unconstrained and constrained RF values therefore reflect the model biases in the local albedo response to a present-day conversion from trees to crops/grasses, which have been described in Section 4.2 for a subset of the models considered here. Hence, the constrained global RF estimates from the models using the CLM as a land surface scheme (CCSM4, CESM1-CAM5, CESM1-FASTCHEM, NorESM1-M) and those from the MPI suite (MPI-ESM-LR, MPI-ESM-MR, MPI-ESM-P) are less negative than the unconstrained estimates by 0.02, respectively 0.06-0.07 W/m^2, reflecting the fact that these models overestimate the albedo increase by this land cover transition. On the other hand, the low albedo response exhibited by MIROC5 in snow-covered regions can be related to the more negative RF (by 0.02W/m^2) obtained for this model after constraining it with the observational data from D18. Similarly, the mix of albedo decreases and increases following a present-day transition from trees to crops/grasses that have been identified for MIROC-ESM can also be linked to the fact that the global reconstructed RF equals zero for this model, whereas it reaches -0.29W/m^2 after applying the same observational constraint. Our results also suggest that the albedo change following a transition from trees to crops/grasses simulated by GFDL-CM3 and GFDL-ESM2 is sensibly lower than in the observations from D18, as the constrained estimates are more negative that the constrained ones by as much as 0.09-0.1 W/m^2 for these two models. We identify the opposite behaviour for HadGEM2-ES, for which the unconstrained global RF of -0.01 W/m^2 is reduced to approximately zero once the observational constraint is applied. Lastly, the constrained and unconstrained estimates of the IPSL-CM5A-LR and IPSL-CM5A-MR models are very similar, revealing an albedo response to a conversion between trees and crops/grasses that is close to the observed values.

Although it solely reflects the model spread in the historical conversion rates between trees and crops/grasses $lcc_{tr \to cg}$, the dispersion between the constrained estimates of the global RF is higher than between the unconstrained ones (Figure 13). This is due to two models in particular, for which the $lcc_{tr \to cg}$ values are outliers among the whole set of models, but which at the same time exhibit significant biases in their albedo response to these land cover changes. Thus, in the HadGEM2-ES model the historical conversion rates from trees to crops/grasses are approximately equal to zero everywhere on the globe (Figure S5), hence the corresponding constrained global RF too. However, because the albedo sensitivity to a transition from trees to crops/grasses of this model is stronger than in the observations, the unconstrained RF is slightly more negative (and reaches -0.01W/m^2). The unconstrained RF equals zero for MIROC-ESM, which is in line with a globally averaged albedo

https://doi.org/10.5194/esd-2019-94
Preprint. Discussion started: 2 April 2020


Earth System Dynamics Discussions

response to transitions between trees and crops/grasses that is also equal to zero, as described above in this Section. In contrast, this model also exhibits the strongest constrained estimate (with -0.29 W/m^2) because of the strong historical conversion rates it simulates, which exceed 50% over large areas of Australia, North America, southeastern Brazil, Central Asia and southern Africa.

The extremely low, respectively high historical conversion rates from trees to crops/grasses in HadGEM2-ES and MIROC-ESM cast doubt on the global RF obtained for these two models. In Figure 13 we therefore also show the model spread after omission of the maximum and minimum values of both the unconstrained and constrained RF estimates. It is reduced from 0.2 to 0.12 W/m^2 after applying the observational constraint, which also leads to a slightly more negative model mean value (-0.11 W/m^2 instead of -0.07, note that the models including the same land surface scheme and land cover maps are considered as just one model for the computation of the mean).

For most CMIP5 models, our reconstructions indicate that the historical impact of conversions between trees and crops/grasses on albedo is very similar to that arising from all changes in tree cover (i.e., also including for example the replacement of trees by shrubs and bare soil, or vice-versa, see Figures S6-20). Moreover, we also find a similar effect for albedo variations from all land-cover changes (i.e., also including transitions between shrubs, crops/grasses and bare soil) by comparing experiments with and without the land-cover forcing, available for four of the analysed models (CanESM2, CCSM4, GFDL-ESM2 and IPSL-CM5A-LR, see Figures S6, S7, S11 and S13). HadGEM2-ES is a notable exception (Figure S12), because it overall exhibits a decrease in tree cover comparable to that of other models, but which is not compensated by increases in the area covered by crops/grasses, shrubs or bare soil (not shown). Consequently, the reconstructed method does not capture the full RF from historical land-cover changes for this model. Since it solely considers the transition between trees and crops/grasses, this method likely also slightly overestimates the RF for MPI-ESM-LR, MPI-ESM-MR and MPI-ESM-P (Figures S17-S19), because these three models represent expansion of both forest and crops/grasses over high latitudes. Despite these limitations, our analysis shows that the reconstructed RF from historical transitions between trees and crops/grasses are overall good approximations of the RF from all land-cover changes for most of the analysed CMIP5 models (see also Figure S21).

6 Discussion and conclusions

The conclusions that can be drawn from the presented analysis are manifold. First, we introduced a methodology to derive the albedo of trees and crops/grasses from Earth System model simulations that only provide mean albedo values over grid cells containing a mix of land cover classes. This “reconstruction” method employs multi-linear regressions to disentangle local information on land cover and albedo within moving windows (“big boxes”) encompassing several grid cells. It assumes that spatial albedo variations between neighbouring trees and crops/grasses within a big box are good proxies of the potential albedo change arising from a transition between these two land cover classes. We then demonstrated that the methodology gives estimates of the albedo of trees and crops/grasses that are close to the reference values provided at the

https://doi.org/10.5194/esd-2019-94
Preprint. Discussion started: 2 April 2020


Earth System Dynamics Discussions

sub-gridcell level in simulations for which this information is available. Consequently, as a second step we reconstructed the present-day albedo of trees and crops/grasses in CMIP5 simulations for thirteen models, and compared the obtained results with reference values from observations. Despite the relatively low spatial coverage of the reconstructed estimates in some models, especially over regions where snow is present, we were able to identify substantial model biases which are significantly higher than the error of the reconstruction method. We found that they are reflected further in the representation of the albedo change induced by a transition between trees and crops/grasses in the same CMIP5 models. Finally, we investigated how such model biases influence the historical albedo change due to transitions between trees and crops/grasses as simulated by CMIP5 models, as well as the associated Radiative Forcing. To do so, we used a similar reconstruction methodology, already employed in previous studies, to assess how albedo has been modified as a result of the replacement of trees by crops/grasses since pre-industrial times in fifteen CMIP5 models (including most of those analysed in the previous step). We then derived the associated historical RF using a simple empirically based radiative kernel parametrisation. An observational constrain was also applied to these purely model-based estimates, by replacing the reconstructed albedo response to a conversion from trees to crops/grasses in the models by that of the observational dataset previously used for the model evaluation. The comparison of the unconstrained and observation-constrained RF in the individual models revealed differences reflecting some of the model biases that we had previously described. Moreover, if one omits the influence of two model outliers which have extremely low or high historical conversion rates between trees and crops/grasses, the model spread diminishes and the model mean value is slightly more negative due to the application of the observational constrain, overall leading to a mean estimate of -0.11 W/m^2 (between -0.04 and -0.16) for the RF due to the historical replacement of trees by crops/grasses. Considering all variations in tree cover or even all land-cover changes gives very similar results, because of the simplified representation of land cover in CMIP5 models.

Our RF estimates are therefore directly comparable with those from previous model-based studies, although these considered the effect of all types of land-cover changes. In particular, the IPCC AR5 states that it is very likely that land use change since preindustrial times led to an increase of the Earth albedo with a RF of -0.15W/m^2 (Figure 13), thereby suggesting that the climate model-based studies from Betts *et al.* (2007), E. L. Davin, de Noblet-Ducoudré and Friedlingstein (2007), and Pongratz *et al.* (2009) – which provided numbers closer to -0.2 W/m^2 – had overestimated the simulated albedo response to historical land-cover changes (Myhre *et al.*, 2013). Although our study reveals that such an overestimation is not systematic in the analysed CMIP5 models, it still suggests that the RF from historical land-cover changes is at the lower end of the range provided by AR5 (i.e., rather less negative than its best estimate). Our model mean result is very close to that of Myhre, Kvalevåg and Schaaf (2005), who also constrained past albedo changes with satellite data and found a RF of -0.09 W/m^2, but considered all LCC since pre-agricultural times.

The remaining spread in our constrained RF estimates directly reflects the differences in the simulated historical conversion rates from trees to crops/grasses. It illustrates the various ways the analysed CMIP5 models interpreted the land use transition maps delivered by the Land Use History a product (LUHa, Hurtt *et al.*, 2011). LUHa gives gridded information on annual transitions between four types of land use (primary land, secondary land, crop and pasture) for the 1500-2005 period,

https://doi.org/10.5194/esd-2019-94
Preprint. Discussion started: 2 April 2020


Earth System Dynamics Discussions

which were derived with the Global Land use Model (GLM) based on historical data. These transitions were especially designed to provide common reference land use trajectories for all historical CMIP5 simulations. The CMIP5 models may have however considered that primary and secondary land were either forests or crops/grasses, or even shrubs or bare soil, depending on the land cover distributions that were prescribed or simulated in a given region or under a given climate. These different interpretations of common land use input data contribute substantially to the spread in the albedo variations due to historical land-cover changes, a result which had already been identified among the models participating to the LUCID project (Boisier *et al.*, 2012), as well as more generally for the biogeophysical effect of future land-cover changes on climate in RCP4.5 and RCP8.5 simulations from CMIP5 (Brovkin *et al.*, 2013; Davies-Barnard *et al.*, 2014; Di Vittorio *et al.*, 2014). Solutions have been put forward to reduce the room for interpretation of the imposed land cover forcing in future model intercomparison efforts, such as a direct coupling between the Integrated Assessment Models producing the land cover scenarios and the Earth System Models (Di Vittorio *et al.*, 2014), or the provision of more detailed land cover information (including the land cover fractions allocated to several specific land-use states) in the frame of CMIP6 (Lawrence *et al.*, 2016). Nevertheless, a common dataset for land cover is still subject to uncertainties in land cover reconstructions, as Schmidt *et al.* (2012) have pointed at significant differences between those from Kaplan *et al.* (2011), Pongratz *et al.* (2008) and the HYDE3.1 dataset on which the LUHa product is based (Klein Goldewijk *et al.*, 2011).

A few more limitations need to be kept in mind when interpreting the findings presented in this study. For example, the albedo sensitivity to deforestation was stronger in pre-industrial times, when the background climate was colder and snow extended over larger land areas. Although Boisier *et al.* (2012) and de Noblet-Ducoudré *et al.* (2012) have shown that changes in background climate have had a very limited impact on the regionally averaged LCC-induced albedo changes, re-calculating the observation-constrained RF with pre-industrial albedo sensitivities may give more negative values, especially locally over high-latitude regions. This interplay between different climate drivers can however not be captured with the RF framework, which assumes that their effects are additive (Myhre *et al.*, 2013). It is also of limited use to investigate the impact of land-cover changes on other climate variables than albedo, as it cannot represent their non-radiative biogeophysical effects (i.e., that solely affect the partitioning between latent and sensible heat fluxes). Moreover, in this study we have focused our attention on local LCC-induced albedo changes, although those also led to an important remote cooling in global-scale deforestation experiments conducted with the IPSL model (Davin and de Noblet-Ducoudré, 2010).

In conclusion, we demonstrated the suitability of a new methodology to extract the albedo of trees and crops/grasses in ESM simulations that only provide mean albedo values over grid cells containing a diversity of land cover types. After applying it to historical CMIP5 simulations, we identified significant model biases in the representation of the albedo of both trees and crops/grasses, as well as the albedo change arising from a transition between these two land cover types. Additionally, we reconstructed local albedo modifications due to historical LCC. Since these reconstructions are affected by model biases, we used the observed albedo response to transitions between trees and crops/grasses to derive an observation-constrained RF of historical LCC in CMIP5 models. Compared to IPCC AR5 estimates, our results point at a slightly less strong global mean RF, with some remaining uncertainty due to the various magnitudes of LCC implemented in the analysed models. With the

https://doi.org/10.5194/esd-2019-94
Preprint. Discussion started: 2 April 2020

release of new ESM simulations within CMIP6 (Eyring *et al.*, 2016), new opportunities arise to assess whether the biases identified in this study have been corrected in the latest generation of ESMs. In that respect, the reconstruction methodology developed for this analysis and which has been implemented as a diagnostic in the ESMValTool v2.0 (Eyring *et al.*, 2019) should allow for a more straightforward model evaluation. Additionally, the new approach to harmonise the forcing from historical LCC in CMIP6 may enable to identify a refined estimate of their RF. We suggest that combining recently released observational evidence and model results as proposed in this study will be useful in this context, in order to further reduce uncertainties on the climate impact of historical LCC on both global and local scales.

References

Alkama, R. and Cescatti, A. (2016) 'Biophysical climate impacts of recent changes in global forest cover', *Science*, 351(6273).

Arino, O. *et al.* (2012) *Global Land Cover Map for 2009 (GlobCover 2009)*, *European Space Agency (ESA) & Université catholique de Louvain (UCL)*. doi: 10.1594/PANGAEA.787668.

Betts, R. A. *et al.* (2007) 'Biogeophysical effects of land use on climate: Model simulations of radiative forcing and large-scale temperature change', *Agricultural and Forest Meteorology*, 142(2–4), pp. 216–233. doi: 10.1016/j.agrformet.2006.08.021.

Boisier, J. P. *et al.* (2012) 'Attributing the impacts of land-cover changes in temperate regions on surface temperature and heat fluxes to specific causes : Results from the first LUCID set of simulations', 117, pp. 1–16. doi: 10.1029/2011JD017106.

Boisier, J. P. *et al.* (2013) 'Inferring past land use-induced changes in surface albedo from satellite observations : a useful tool to evaluate model simulations'. doi: 10.5194/bg-10-1501-2013.

Bright, R. M. and O'halloran, T. L. (2019) 'Developing a monthly radiative kernel for surface albedo change from satellite climatologies of Earth's shortwave radiation budget: CACK v1.0', *Geosci. Model Dev*, 12, pp. 3975–3990. doi: 10.5194/gmd-12-3975-2019.

Brovkin, V. *et al.* (2013) 'Effect of Anthropogenic Land-Use and Land-Cover Changes on Climate and Land Carbon Storage in CMIP5 Projections for the Twenty-First Century', *Journal of Climate*. American Meteorological Society, 26(18), pp. 6859–6881. doi: 10.1175/JCLI-D-12-00623.1.

Cescatti, A. *et al.* (2012) 'Intercomparison of MODIS albedo retrievals and in situ measurements across the global FLUXNET network', *Remote Sensing of Environment*, 121, pp. 323–334. doi: 10.1016/j.rse.2012.02.019.

Chen, L. and Dirmeyer, P. A. (2019) 'Global observed and modelled impacts of irrigation on surface temperature', *International Journal of Climatology*, 39(5), pp. 2587–2600. doi: 10.1002/joc.5973.

Cherubini, F., Bright, R. M. and Strømman, A. H. (2012) 'Site-specific global warming potentials of biogenic CO2 for bioenergy: contributions from carbon fluxes and albedo dynamics', *Environ. Res. Lett*, 7, p. 45902. doi: 10.1088/1748-

9326/7/4/045902.

Davies-Barnard, T. *et al.* (2014) 'Climatic Impacts of Land-Use Change due to Crop Yield Increases and a Universal Carbon Tax from a Scenario Model', *Journal of Climate*, 27, pp. 1413–1424. doi: 10.1175/JCLI-D-13.

Davin, E. L. and de Noblet-Ducoudré, N. (2010) 'Climatic Impact of Global-Scale Deforestation : Radiative versus Nonradiative Processes', pp. 97–112. doi: 10.1175/2009JCLI3102.1.

Davin, Edouard L., de Noblet-Ducoudré, N. and Friedlingstein, P. (2007) 'Impact of land cover change on surface climate: Relevance of the radiative forcing concept', *Geophysical Research Letters*, 34(13). doi: 10.1029/2007GL029678.

Davin, E. L., de Noblet-Ducoudré, N. and Friedlingstein, P. (2007) 'Impact of land cover change on surface climate: Relevance of the radiative forcing concept', *Geophysical Research Letters*, 34(13), p. n/a-n/a. doi: 10.1029/2007GL029678.

Duveiller, G. *et al.* (2018) 'Biophysics and vegetation cover change: A process-based evaluation framework for confronting land surface models with satellite observations', *Earth System Science Data*, 10(3), pp. 1265–1279. doi: 10.5194/essd-10-1265-2018.

Duveiller, G. *et al.* (2020) 'Local biophysical effects of land use and land cover change: towards an assessment tool for policy makers', *Land Use Policy*, 91, p. 104382. doi: 10.1016/j.landusepol.2019.104382.

Duveiller, G., Hooker, J. and Cescatti, A. (2018a) 'A dataset mapping the potential biophysical effects of vegetation cover change', *Scientific Data*. Nature Publishing Groups, 5. doi: 10.1038/sdata.2018.14.

Duveiller, G., Hooker, J. and Cescatti, A. (2018b) 'The mark of vegetation change on Earth's surface energy balance', *Nature Communications*. Springer US, 9(1). doi: 10.1038/s41467-017-02810-8.

Efron, B. (1982) '6. The Infinitesimal Jackknife, the Delta Method and the Influence Function', in *The Jackknife, the Bootstrap and Other Resampling Plans*. Society for Industrial and Applied Mathematics, pp. 37–47. doi: 10.1137/1.9781611970319.ch6.

Eyring, V. *et al.* (2016) 'Overview of the Coupled Model Intercomparison Project Phase 6 (CMIP6) experimental design and organization', *Geoscientific Model Development*, 9(5), pp. 1937–1958. doi: 10.5194/gmd-9-1937-2016.

Eyring, V. *et al.* (2019) 'ESMValTool v2 . 0 – Extended set of large-scale diagnostics for quasi-operational and comprehensive evaluation of Earth system models in CMIP', (November).

Foley, J. A. *et al.* (2005) 'Global consequences of land use', *Science*, pp. 570–574. doi: 10.1126/science.1111772.

Harris, I. *et al.* (2014) 'Updated high-resolution grids of monthly climatic observations - the CRU TS3.10 Dataset', *International Journal of Climatology*, 34(3), pp. 623–642. doi: 10.1002/joc.3711.

Hurtt, G. C. *et al.* (2011) 'Harmonization of land-use scenarios for the period 1500-2100: 600 years of global gridded annual land-use transitions, wood harvest, and resulting secondary lands', *Climatic Change*, 109, pp. 117–161. doi: 10.1007/s10584-011-0153-2.

Kaplan, J. O. *et al.* (2011) 'Holocene carbon emissions as a result of anthropogenic land cover change', *Holocene*, 21(5), pp. 775–791. doi: 10.1177/0959683610386983.

Klein Goldewijk, K. *et al.* (2011) 'The HYDE 3.1 spatially explicit database of human-induced global land-use change over

the past 12,000 years', *Global Ecology and Biogeography*, 20(1), pp. 73–86. doi: 10.1111/j.1466-8238.2010.00587.x.

Kvalevåg, M. M. *et al.* (2010) 'Anthropogenic land cover changes in a GCM with surface albedo changes based on MODIS data', *International Journal of Climatology*, 30(13), pp. 2105–2117. doi: 10.1002/joc.2012.

Lacis, A. A. and Hansen, J. E. (1974) 'A Parameterization for the Absorption of Solar Radiation in the Earth's Atmosphere', *Journal of the Atmospheric Sciences*, 31, pp. 118–133.

Lawrence, D. M. *et al.* (2016) 'The Land Use Model Intercomparison Project (LUMIP) contribution to CMIP6: Rationale and experimental design', *Geoscientific Model Development*, 9(9), pp. 2973–2998. doi: 10.5194/gmd-9-2973-2016.

Lawrence, P. J. and Chase, T. N. (2007) 'Representing a new MODIS consistent land surface in the Community Land Model (CLM 3.0)', *Journal of Geophysical Research*, 112(G1), p. G01023. doi: 10.1029/2006JG000168.

Lejeune, Q. *et al.* (2018) 'Historical deforestation locally increased the intensity of hot days in northern mid-latitudes', *Nature Climate Change*. Springer US, 8(5), pp. 386–390. doi: 10.1038/s41558-018-0131-z.

Lejeune, Q., Seneviratne, S. I. and Davin, E. L. (2017) 'Historical land-cover change impacts on climate: Comparative assessment of LUCID and CMIP5 multimodel experiments', *Journal of Climate*, 30(4), pp. 1439–1459. doi: 10.1175/JCLI-D-16-0213.1.

Lenton, T. M. and Vaughan, N. E. (2009) *The radiative forcing potential of different climate geoengineering options*, *Atmos. Chem. Phys*. Available at: www.atmos-chem-phys.net/9/5539/2009/ (Accessed: 6 December 2019).

Lewis, P. *et al.* (2012) 'The ESA globAlbedo project: Algorithm', *International Geoscience and Remote Sensing Symposium (IGARSS)*, (February 2015), pp. 5745–5748. doi: 10.1109/IGARSS.2012.6352306.

Li, Y. *et al.* (2015) 'Local cooling and warming effects of forests based on satellite observations', *Nature Communications*. Nature Publishing Group, 6, pp. 1–8. doi: 10.1038/ncomms7603.

Mahmood, R. *et al.* (2014) 'Land cover changes and their biogeophysical effects on climate', *International Journal of Climatology*, 34(4), pp. 929–953. doi: 10.1002/joc.3736.

Malyshev, S. *et al.* (2015) 'Contrasting Local versus Regional Effects of Land-Use-Change-Induced Heterogeneity on Historical Climate: Analysis with the GFDL Earth System Model', *Journal of Climate*, 28, pp. 5448–5469. doi: 10.1175/JCLI-D-14-00586.1.

Meier, R. *et al.* (2018) 'Evaluating and improving the Community Land Model's sensitivity to land cover', *Biogeosciences*, 15, pp. 4731–4757. doi: 10.5194/bg-15-4731-2018.

Myhre, G. *et al.* (2013) 'Anthropogenic and Natural Radiative Forcing', in Stocker, T. F. et al. (eds) *Climate Change 2013: The Physical Science Basis. Contribution of Working Group I to the Fifth Assessment Report of the Intergovernmental Panel on Climate Change*. Cambridge, UK and New York, US: Cambridge University Press, p. in press.

Myhre, G., Kvalevåg, M. M. and Schaaf, C. B. (2005) 'Radiative forcing due to anthropogenic vegetation change based on MODIS surface albedo data', *Geophysical Research Letters*, 32(21), p. L21410. doi: 10.1029/2005GL024004.

de Noblet-Ducoudré, N. *et al.* (2012) 'Determining Robust Impacts of Land-Use-Induced Land Cover Changes on Surface Climate over North America and Eurasia : Results from the First Set of LUCID Experiments'. doi: 10.1175/JCLI-D-11-

00338.1.

Oleson, K. W. *et al.* (2013) 'NCAR/TN-503+STR NCAR Technical Note Technical Description of version 4.5 of the Community Land Model (CLM) Coordinating Lead Authors'. Available at: http://library.ucar.edu/research/publish-technote (Accessed: 31 December 2019).

Pitman, A. J. *et al.* (2009) 'Uncertainties in climate responses to past land cover change: First results from the LUCID intercomparison study', *Geophysical Research Letters*, 36(14), pp. 1–6. doi: 10.1029/2009GL039076.

Pongratz, J. *et al.* (2008) 'A reconstruction of global agricultural areas and land cover for the last millennium', *Global Biogeochemical Cycles*, 22(3), p. n/a-n/a. doi: 10.1029/2007GB003153.

Pongratz, J. *et al.* (2009) 'Radiative forcing from anthropogenic land cover change since A.D. 800', *Geophysical Research Letters*, 36(2), p. n/a-n/a. doi: 10.1029/2008GL036394.

Pongratz, J. *et al.* (2010) 'Biogeophysical versus biogeochemical climate response to historical anthropogenic land cover change', *Geophysical Research Letters*, 37(8), pp. 1–5. doi: 10.1029/2010GL043010.

Ramankutty, N. and Foley, J. A. (1999) 'Estimating historical changes in global land cover: Croplands from 1700 to 1992', *Global Biogeochemical Cycles*, 13(4), pp. 997–1027. doi: 10.1029/1999GB900046.

Schaaf, C. B. *et al.* (2002) 'First operational BRDF, albedo nadir reflectance products from MODIS', *Remote Sensing of Environment*, 83(1–2), pp. 135–148. doi: 10.1016/S0034-4257(02)00091-3.

Schmidt, G. a. *et al.* (2012) 'Climate forcing reconstructions for use in PMIP simulations of the Last Millennium (v1.1)', *Geoscientific Model Development*, 5(1), pp. 185–191. doi: 10.5194/gmd-5-185-2012.

Soden, B. J. *et al.* (2008) 'Quantifying Climate Feedbacks Using Radiative Kernels'. doi: 10.1175/2007JCLI2110.1.

Taylor, K. E., Stouffer, R. J. and Meehl, G. a. (2012) 'An Overview of CMIP5 and the Experiment Design', *Bulletin of the American Meteorological Society*, 93(4), pp. 485–498. doi: 10.1175/BAMS-D-11-00094.1.

Di Vittorio, A. V *et al.* (2014) 'From land use to land cover: restoring the afforestation signal in a coupled integrated assessment-earth system model and the implications for CMIP5 RCP simulations', *Biogeosciences*, 11, pp. 6435–6450. doi: 10.5194/bg-11-6435-2014.

Winckler, J. *et al.* (2019) 'Nonlocal Effects Dominate the Global Mean Surface Temperature Response to the Biogeophysical Effects of Deforestation', *Geophysical Research Letters*, 46(2), pp. 745–755. doi: 10.1029/2018GL080211.

Winckler, J., Reick, C. H. and Pongratz, J. (2017) 'Robust identification of local biogeophysical effects of land-cover change in a global climate model', *Journal of Climate*, 30(3), pp. 1159–1176. doi: 10.1175/JCLI-D-16-0067.1.

https://doi.org/10.5194/esd-2019-94
Preprint. Discussion started: 2 April 2020

Earth System Dynamics
Discussions
Open Access
EGU

RMSE	trees	Crops/grasses	Trees to crops/grasses
July	0.009	0.010	0.019
January	0.019	0.013	0.025

Table 1: Root Mean Square Errors associated to the reconstruction of the albedo of trees, crops/grasses and the transition between these two land cover classes, for the months of July and January.

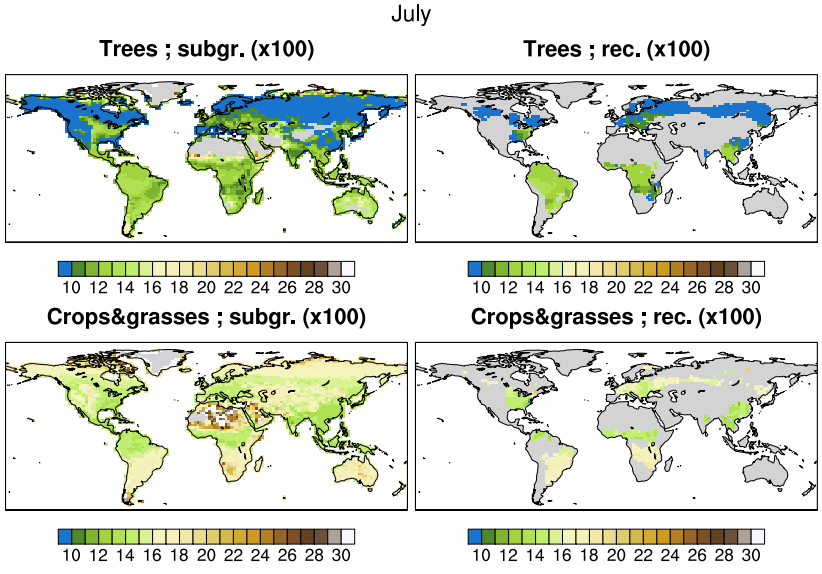

Figure 1: Subgrid (left) and reconstructed (right) estimates of the albedo of trees (upper row) and crops/grasses (lower row) in the CLM4.5 simulations, for the month of July. Note that absolute differences have been multiplied by 100 to facilitate readability.

https://doi.org/10.5194/esd-2019-94
Preprint. Discussion started: 2 April 2020

Earth System Dynamics
Discussions
Open Access
EGU

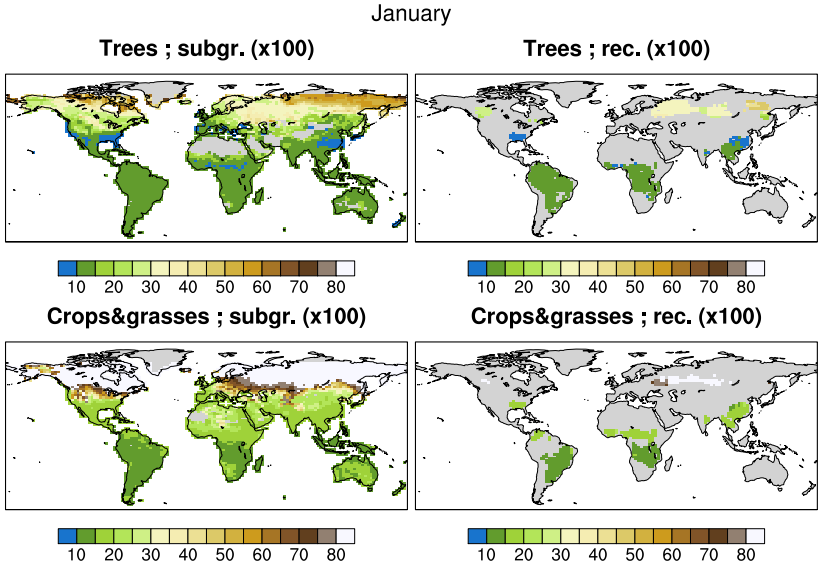

Figure 2: Same as Figure 1, but for the month of January. Note that the scale is different.

675

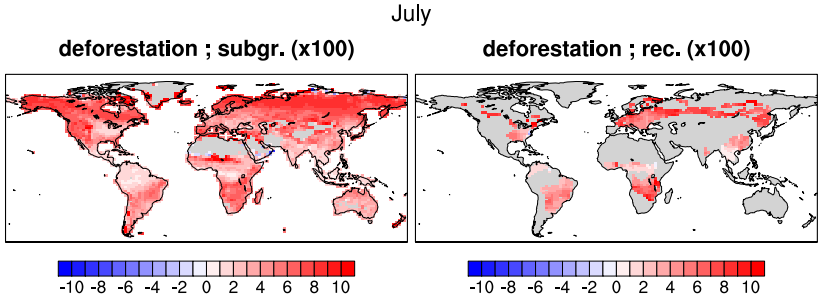

Figure 3: Subgrid (left) and reconstructed (right) estimates of the albedo change associated to a transition from trees to crops/grasses in the CLM4.5 simulations, for the month of July. Note that absolute differences have been multiplied by 100 to facilitate reading.

https://doi.org/10.5194/esd-2019-94
Preprint. Discussion started: 2 April 2020

Earth System Dynamics
Discussions
Open Access
EGU

680

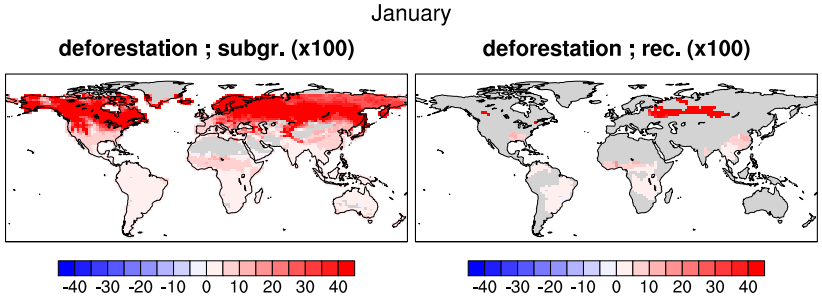

Figure 4: Same as Figure 3, but for the month of January. Note that the scale is different.

https://doi.org/10.5194/esd-2019-94
Preprint. Discussion started: 2 April 2020

Earth System Dynamics
Discussions
Open Access
EGU

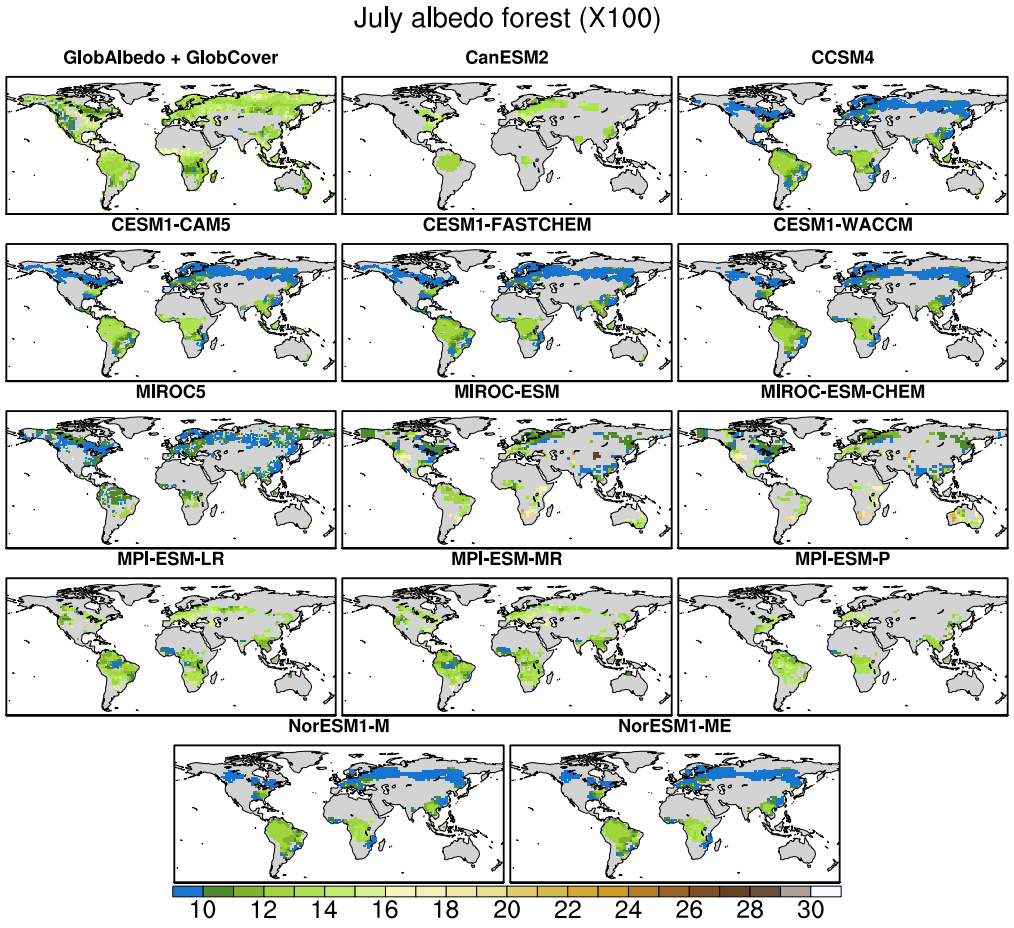

685 **Figure 5: July albedo of trees retrieved from the combination of the observational data GlobAlbedo and GlobCover (top-left corner) and in the analysed CMIP5 models. Note that the albedo values have been multiplied by 100 to facilitate readability.**

https://doi.org/10.5194/esd-2019-94
Preprint. Discussion started: 2 April 2020

Earth System Dynamics
Discussions
Open Access
EGU

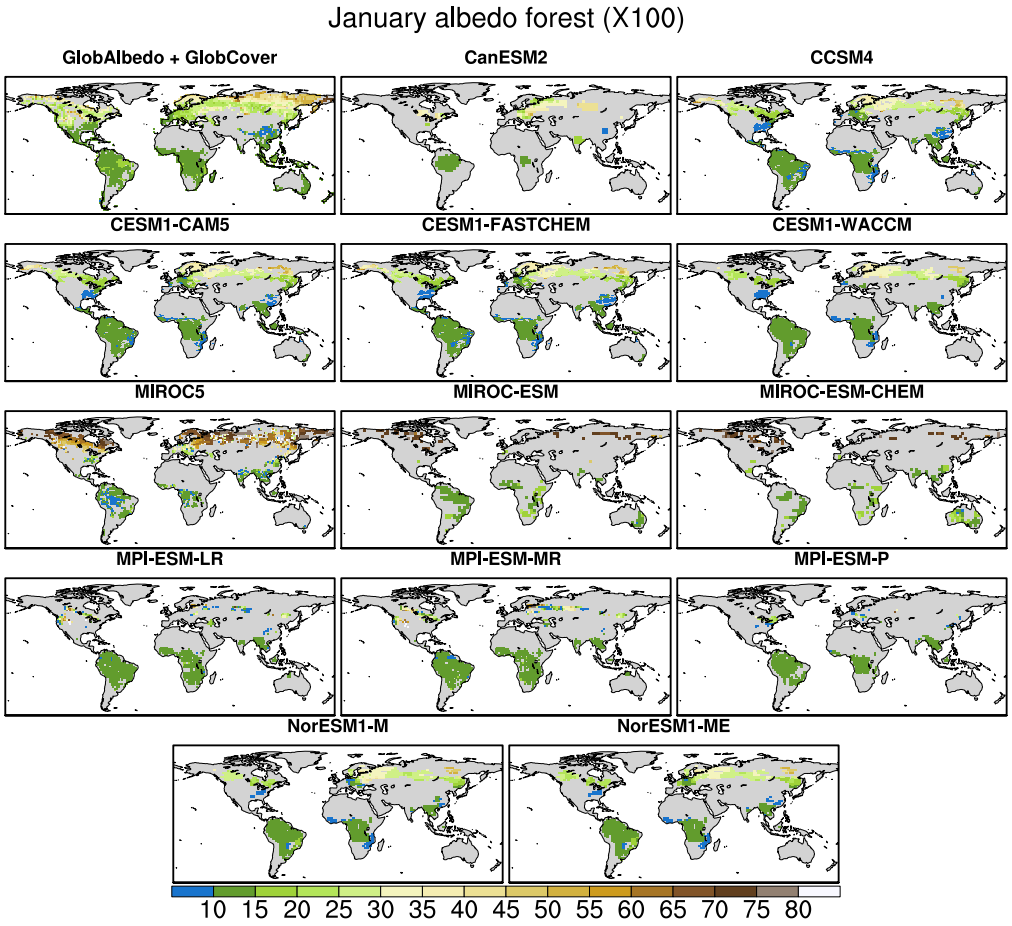

Figure 6: Same as Figure 5, but for the month of January. Note that the scale is different.

https://doi.org/10.5194/esd-2019-94
Preprint. Discussion started: 2 April 2020

Earth System Dynamics
Discussions
Open Access
EGU

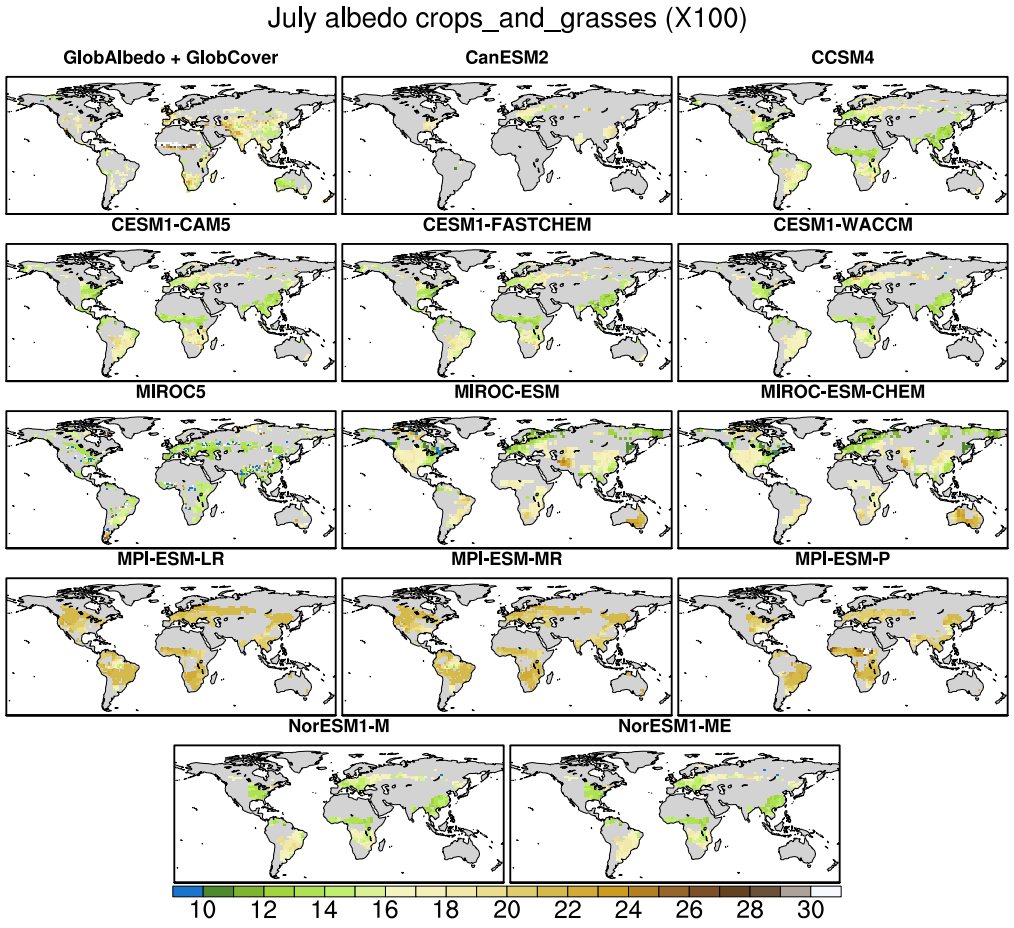

690 **Figure 7: July albedo of crops/grasses according to the combined observational data GlobAlbedo and GlobCover (top-left corner) and in the analysed CMIP5 models.**

https://doi.org/10.5194/esd-2019-94
Preprint. Discussion started: 2 April 2020

Earth System Dynamics
Discussions
Open Access
EGU

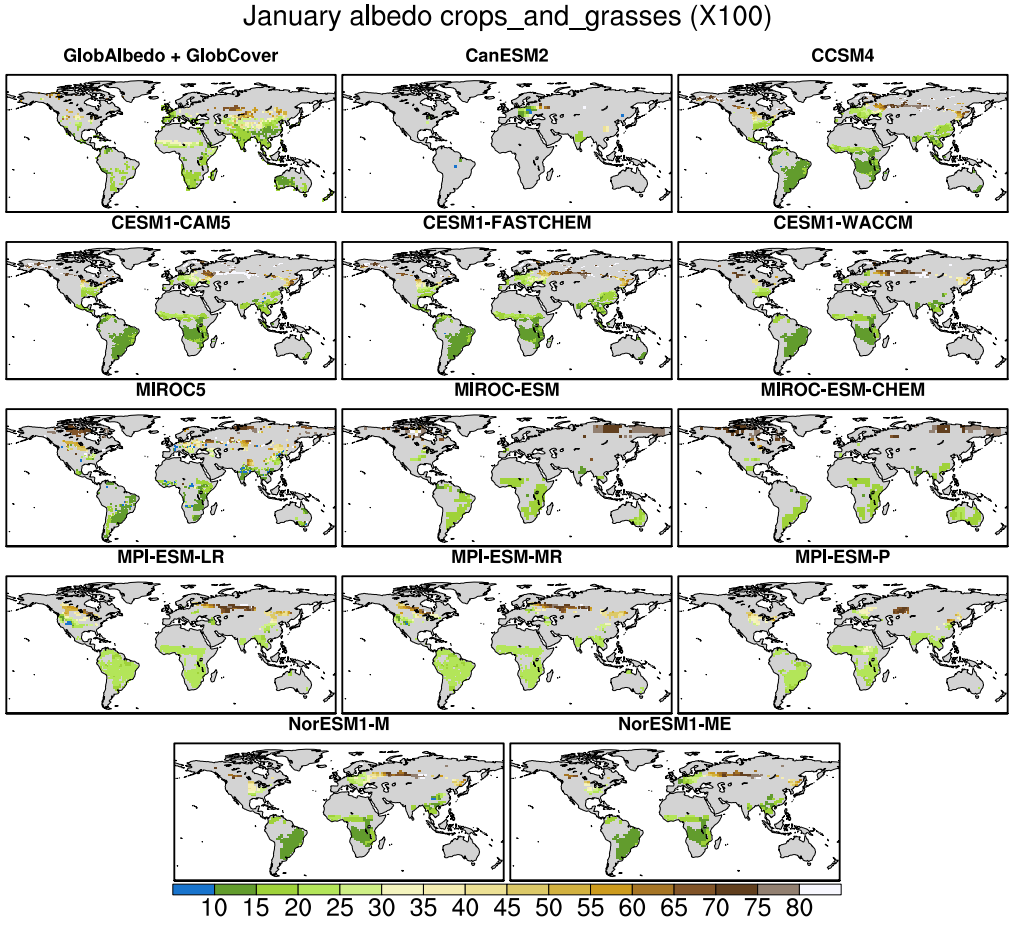

Figure 8: Same as Figure 7, but for the month of January. Note that the scale is different.

https://doi.org/10.5194/esd-2019-94
Preprint. Discussion started: 2 April 2020

Earth System Dynamics
Discussions
Open Access
EGU

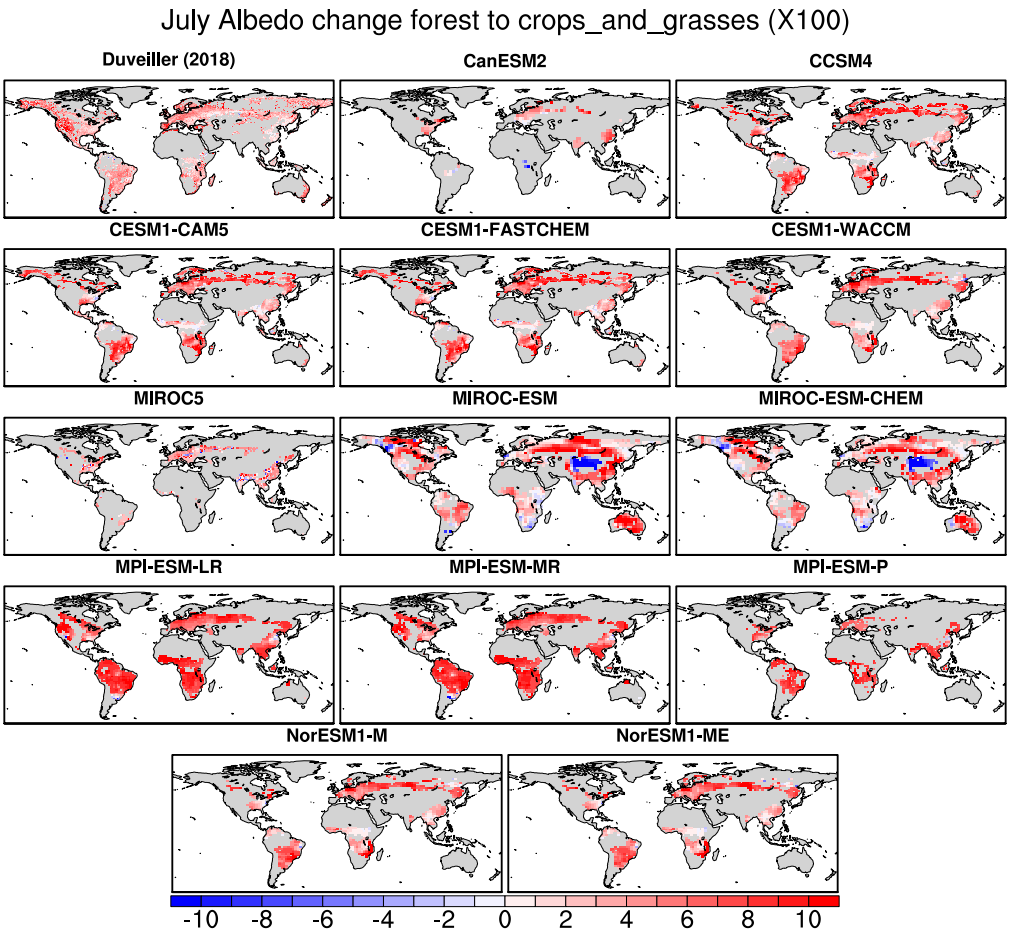

695 **Figure 9: July albedo change associated to a transition from trees to crops/grasses according to the observational dataset of** (Duveiller, Hooker and Cescatti, 2018) **(top-left corner) and in the analysed CMIP5 models.**

https://doi.org/10.5194/esd-2019-94
Preprint. Discussion started: 2 April 2020

Earth System Dynamics
Discussions
Open Access
EGU

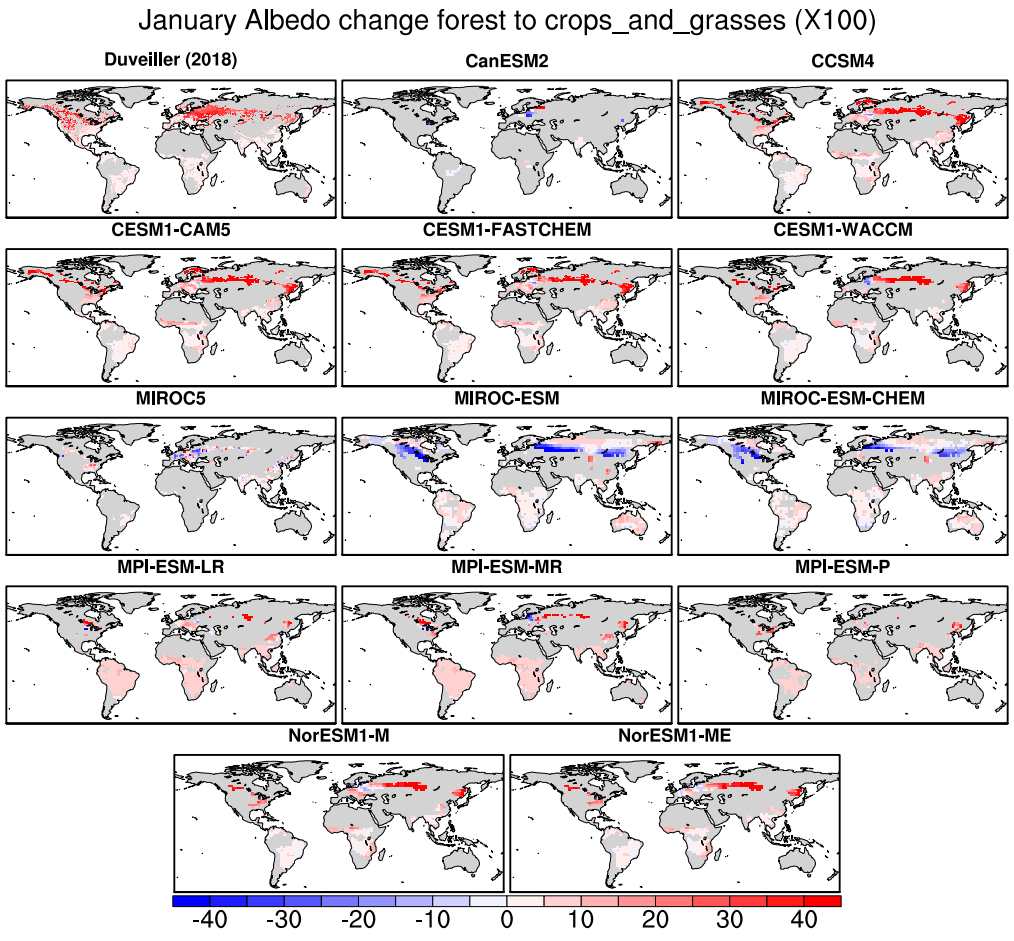

Figure 10: Same as Figure 9, but for January. Note that the scale is different.

https://doi.org/10.5194/esd-2019-94
Preprint. Discussion started: 2 April 2020

Earth System Dynamics
Discussions
Open Access
EGU

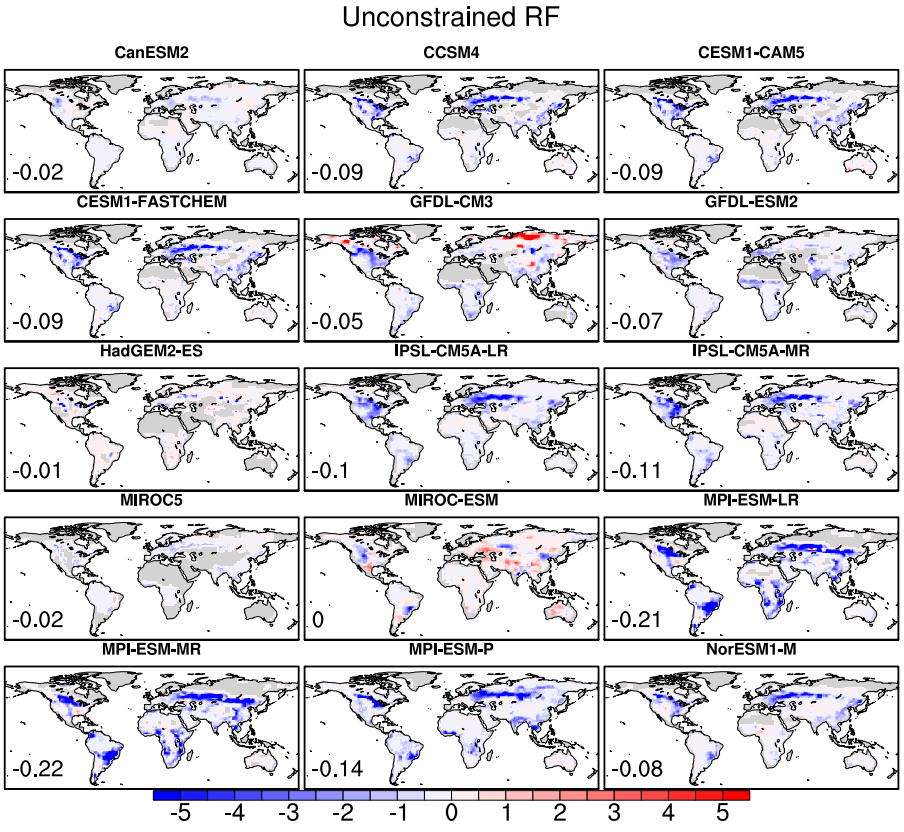

Figure 11: Radiative Forcing from historical deforestation in the analysed CMIP5 models (in W/m^2), obtained by applying the reconstruction method. The numbers in the bottom-left corner of each map indicate the global mean Radiative Forcing from historical deforestation.

https://doi.org/10.5194/esd-2019-94
Preprint. Discussion started: 2 April 2020

Earth System Dynamics
Discussions
Open Access
EGU

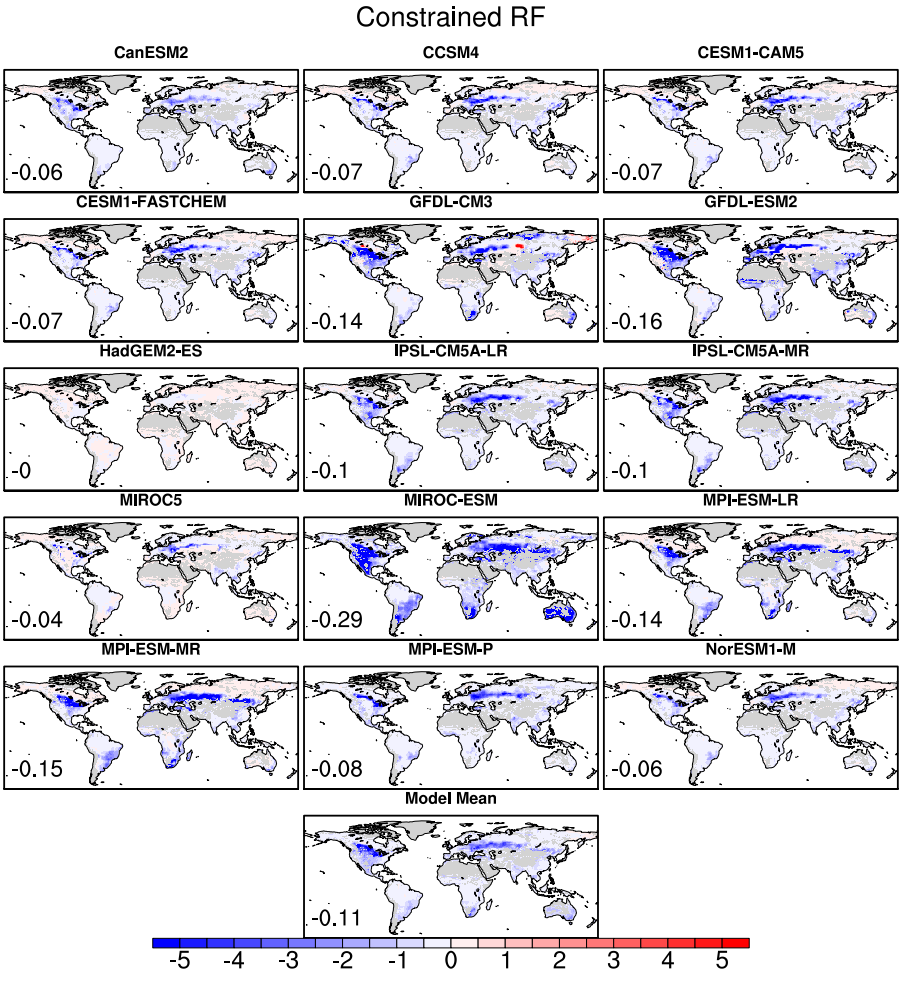

Figure 12: Observation-constrained Radiative Forcing from historical deforestation in the analysed CMIP5 models (in W/m^2). The numbers in the bottom-left corner of each map indicate the global mean Radiative Forcing. To compute the Model Mean, if

https://doi.org/10.5194/esd-2019-94
Preprint. Discussion started: 2 April 2020

Earth System Dynamics
Discussions
Open Access
EGU

several CMIP5 models contain the same Land Surface Model they were attributed a lower weight so that the sum of these weights equal 1.

https://doi.org/10.5194/esd-2019-94
Preprint. Discussion started: 2 April 2020

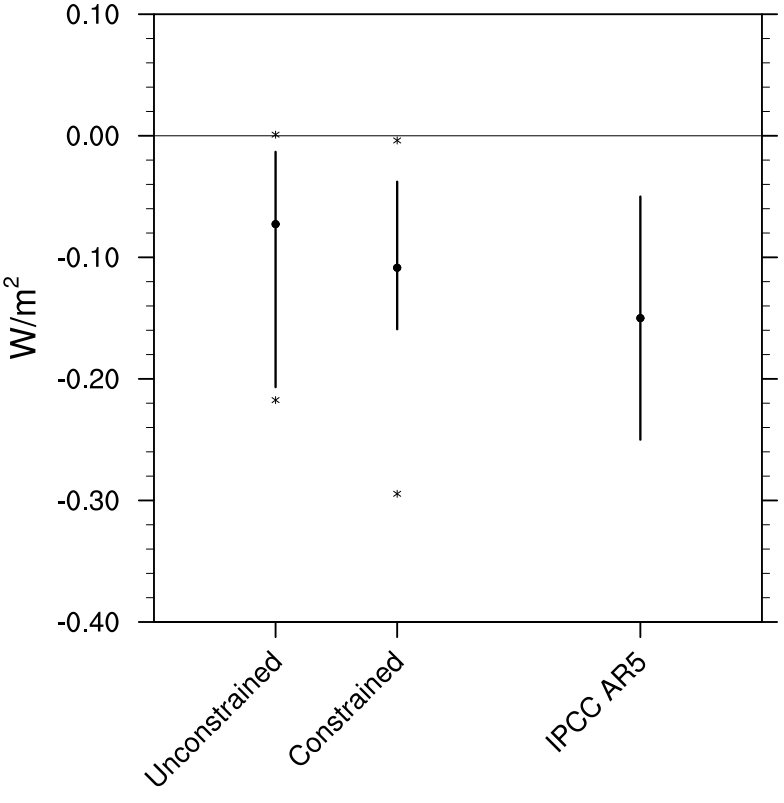

Figure 13: Spread in the unconstrained (left bar) and observation-constrained (middle bar) estimates of the global Radiative Forcing from historical deforestation for the CMIP5 models shown in Figures 11 and 12 (in W/m^2), as well as the IPCC AR5

https://doi.org/10.5194/esd-2019-94
Preprint. Discussion started: 2 April 2020

estimate of the global Radiative Forcing from historical land-use changes (mean estimate and spread as in (Myhre *et al.*, 2013)**). The dots on the left and middle bars show the model mean results for the unconstrained and observation-constrained estimates, respectively, the asterisks mark the lowest and highest value for each category, while the lengths of the bars indicate the spread between the first and ninth deciles.**

715